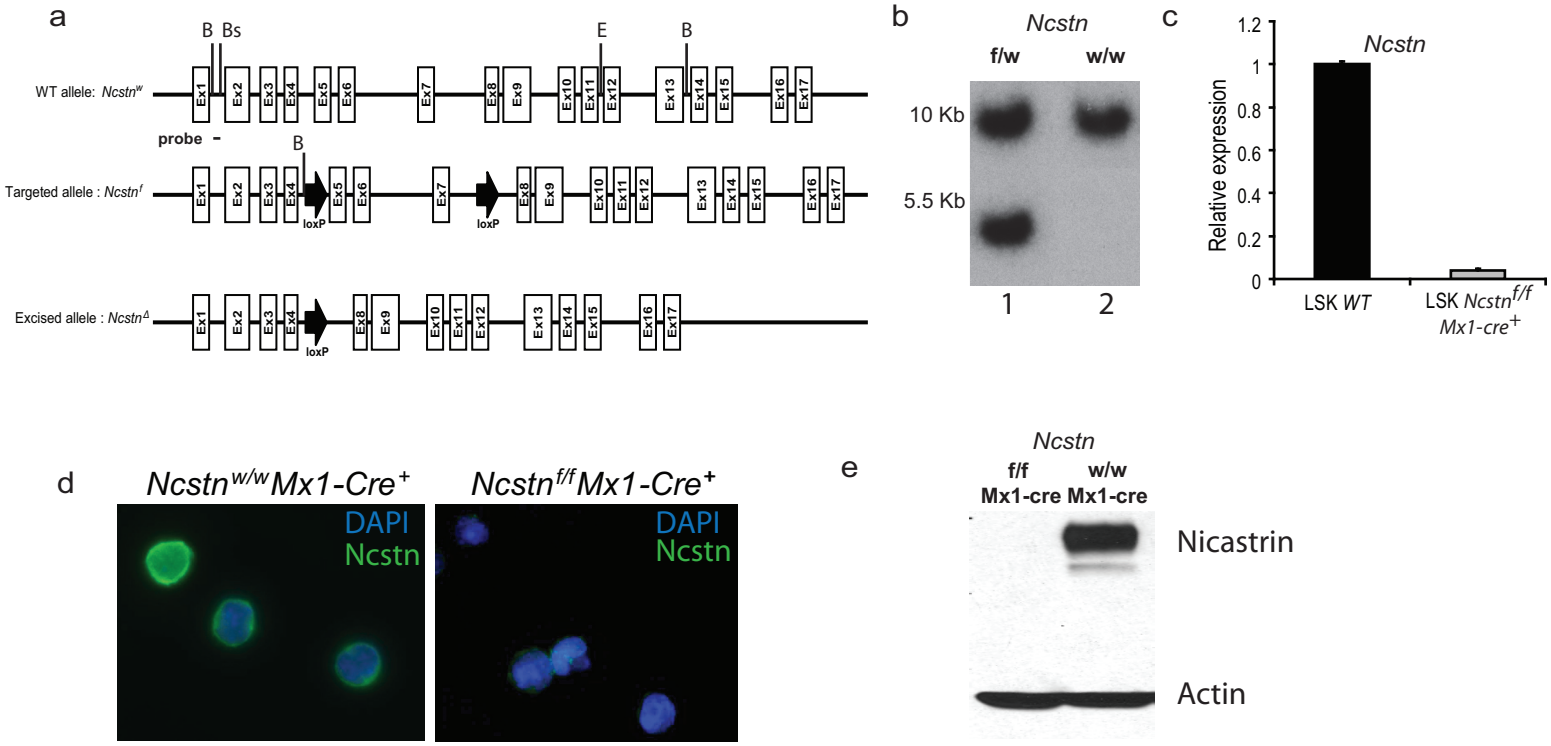

Supplemental Figure 1: Generation of a conditional Ncstn allele.

a, Targeting strategy of the Nicastrin (Ncstn) allele. Restriction sites used for targeting and screening are shown. B: BamHI, Bs: BsrGI, E: EcoRI. **b,** Southern Blot analysis of DNA isolated from targeted ES cells. Genomic DNA was digested with BamHI restriction enzyme, separated in an agarose gel, and hybridized with a 32P-labeled probe specific for the region indicated in a. Lane 2, untargeted control ES cell clone; lane 1, targeted ES cell clone used for generation of the knock-out mice. **c,** Quantitative PCR for Ncstn on sorted LSK from Ncstn$^{f/f}$ Mx1-cre+ and WT littermate. **d,** Immuno-fluorescence for Ncstn protein on sorted LSK showing that Ncstn deletion induces a complete loss of Ncstn protein. **e,** Western Blot analysis of total bone marrow from Ncstn$^{w/w}$ Mx1-cre+ and Ncstn$^{f/f}$ Mx1-cre+ mice 2 weeks after polyI-polyC injections.

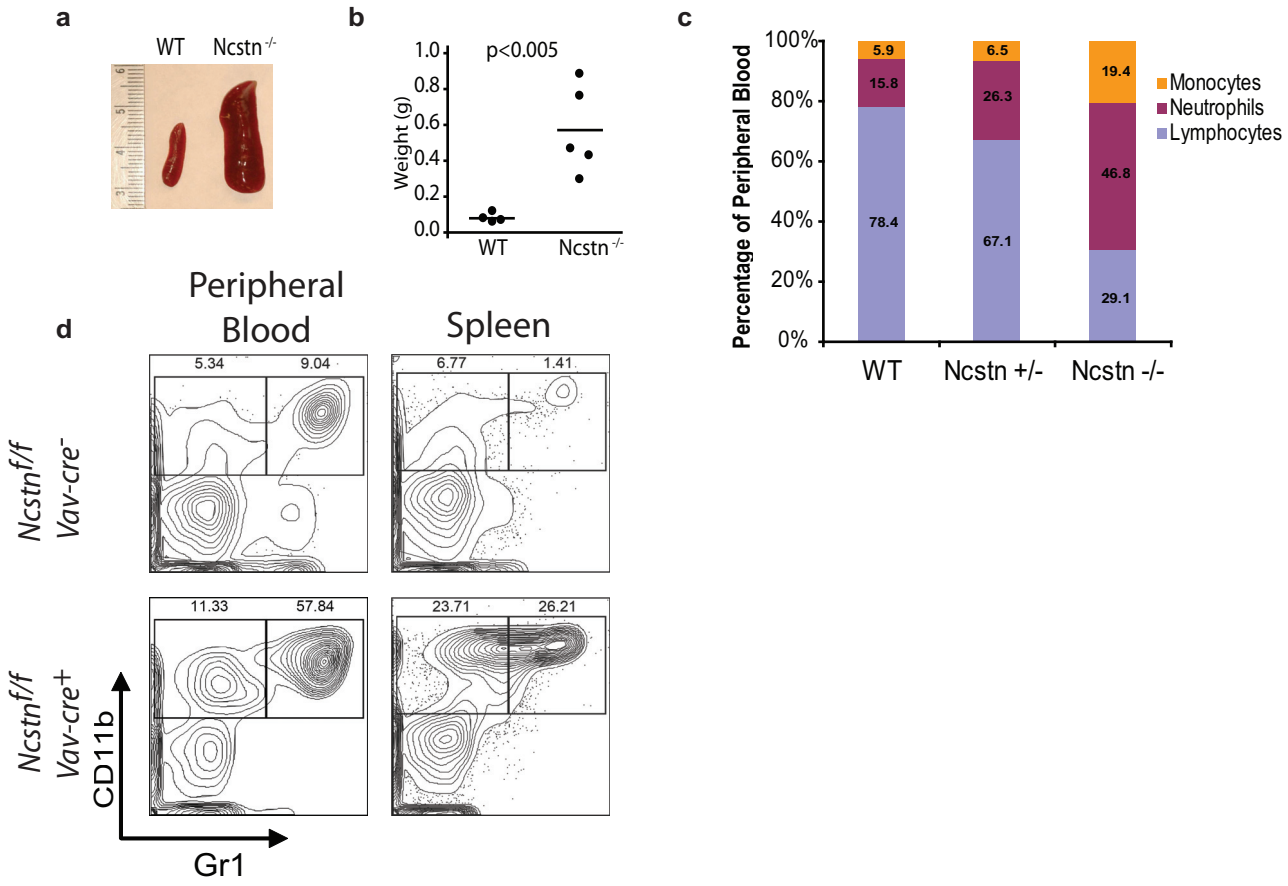

Figure 2: Ncstn deficiency leads to CMML-like disease.

a-b, Massive enlargement of the spleen in Ncstn$^{-/-}$ mice (right) compared to an age-matched littermate controls (left). The absolute weight of the spleens is shown in b. **c,** relative percentages of white blood cell populations in peripheral blood of the denoted animal genotypes (n=10 for each genotype). **d,** Flow cytometric analysis of Gr1/CD11b myeloid cells from the spleen, and peripheral blood of control and Ncstn$^{f/f}$ Vav-cre+ littermate animals.

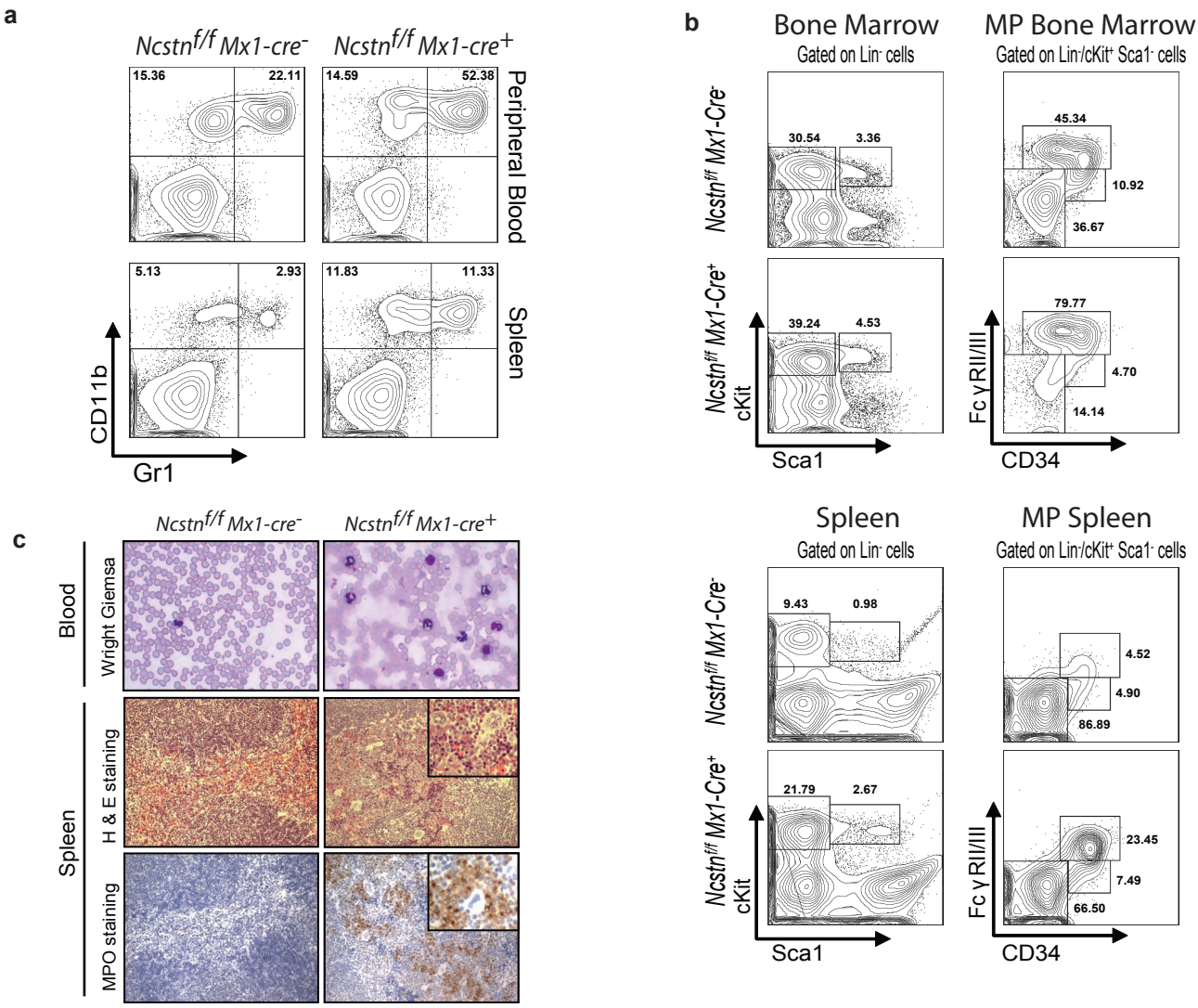

Supplemental Figure 3: Mx1cre-mediated Ncstn deletion leads to CMML-like disease and an expansion of the GMP progenitor population.

a, Flow cytometric analysis of Gr1/CD11b myeloid cells from the spleen, and peripheral blood of 6-week-old control and Ncstn$^{f/f}$ Mx1-cre+ littermate animals. **b,** Detailed FACS analysis of bone marrow LSK and myeloid progenitors (MP: Lin-/c-Kit+/Sca-1-/CD34/FcgRII/III populations of Ncstn$^{f/f}$ Mx1-cre+ and Ncstn$^{f/f}$ Mx1-cre- littermates. Both bone marrow and spleen populations are shown. **c,** Wright-Giemsa staining of peripheral blood smears showing expansion of mature-appearing monocytes and granulocytes in Ncstn$^{f/f}$ Mx1-Cre+ mice compared to control littermates (Upper panel). H&E staining of spleen showing red pulp expansion and signs of extramedullary hematopoiesis (middle panel). Myeloperoxydase (MPO) staining of spleen sections shows massive invasion by myeloid cells (lower panel).

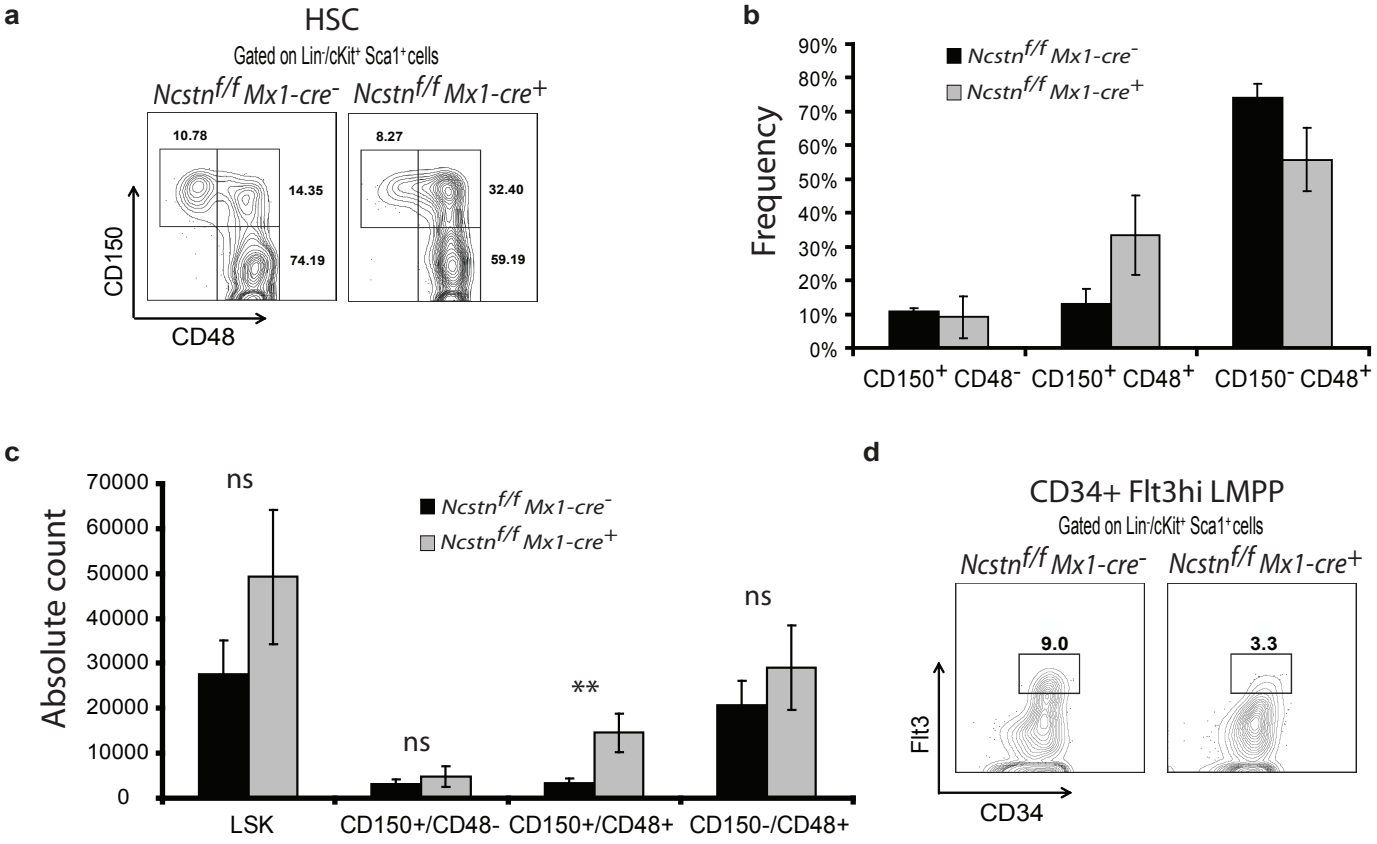

Supplemental Figure 4: Effects of Ncstn deletion in the most primitive LSK subsets.
a, SLAM-marker (CD150, CD48) breakdown of the LSK compartment in Ncstn$^{f/f}$ Mx1-cre+ and control littermates. **b,** Percentages and **c,** absolute numbers of each of the indicated populations demonstrating a specific increase of the CD150+48+ subset (mean±S.D., n=6) . **d,** Quantification of FLT3^{hi} LSK subset (LMPP) in Ncstn$^{f/f}$ Mx1-cre+ and control littermates.

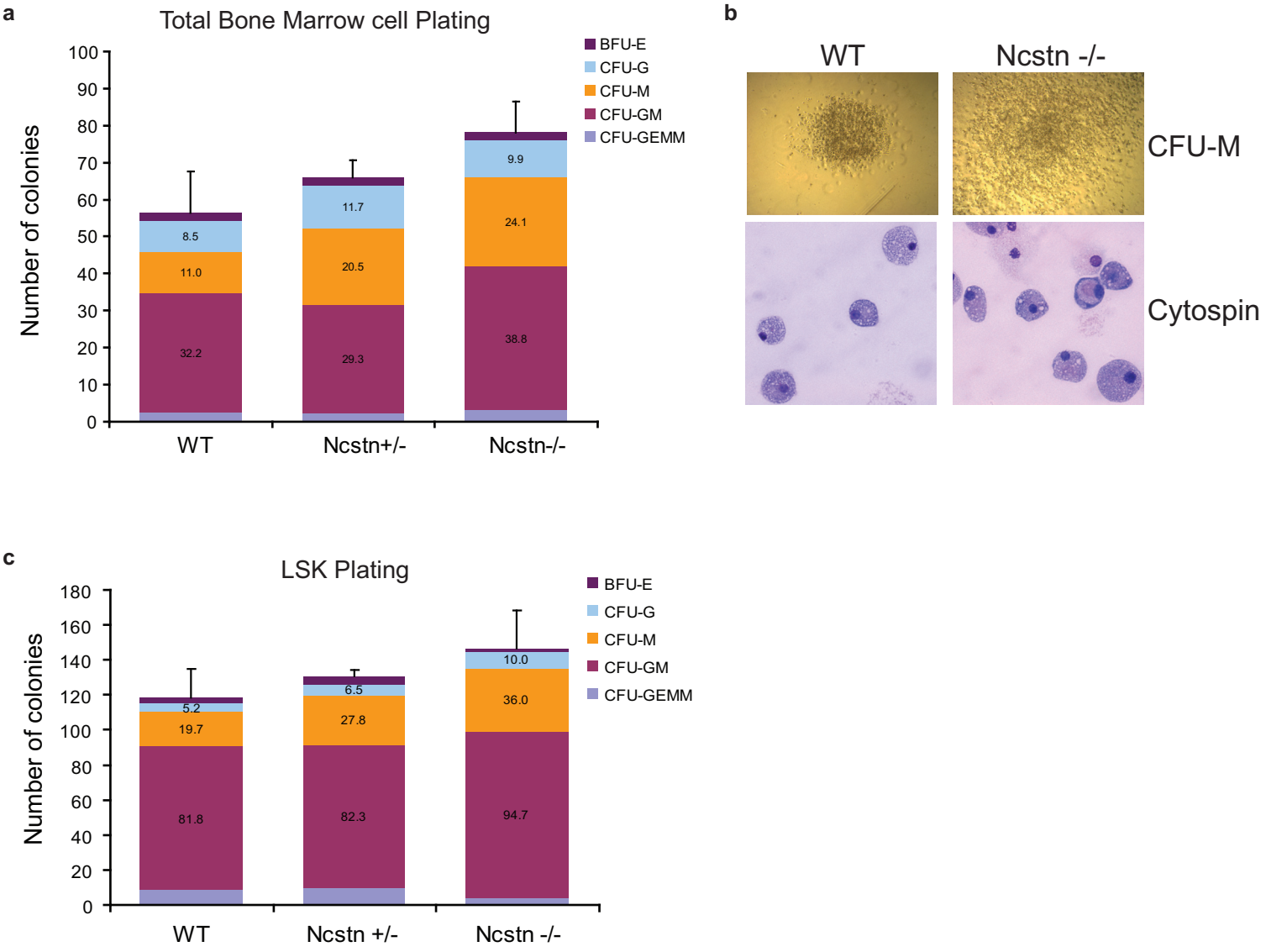

Supplemental Figure 5: Ncstn deletion affects progenitor in vitro differentiation.
a, Culture of total bone marrow cells on methylcellulose. Colonies were counted and phenotypically identified at day 10 after the beginning of the culture. **b,** Representative picture and cytospins of CFU-M showing differences in size (upper panels) and macrophage-like morphology (lower panels) at day 10 after the initiation of culture. **c,** An identical in vitro culture as in a is shown but the starting population is sorted LSK cells from Ncstn$^{f/f}$ Vav1-cre+, Ncstn$^{f/wt}$ Vav1-cre+ and control littermate mice. All experiments show averaging of counts of cells from 3 individual mice in each genotype. Each plating was ralized in triplicate (mean±S.D., n=3)

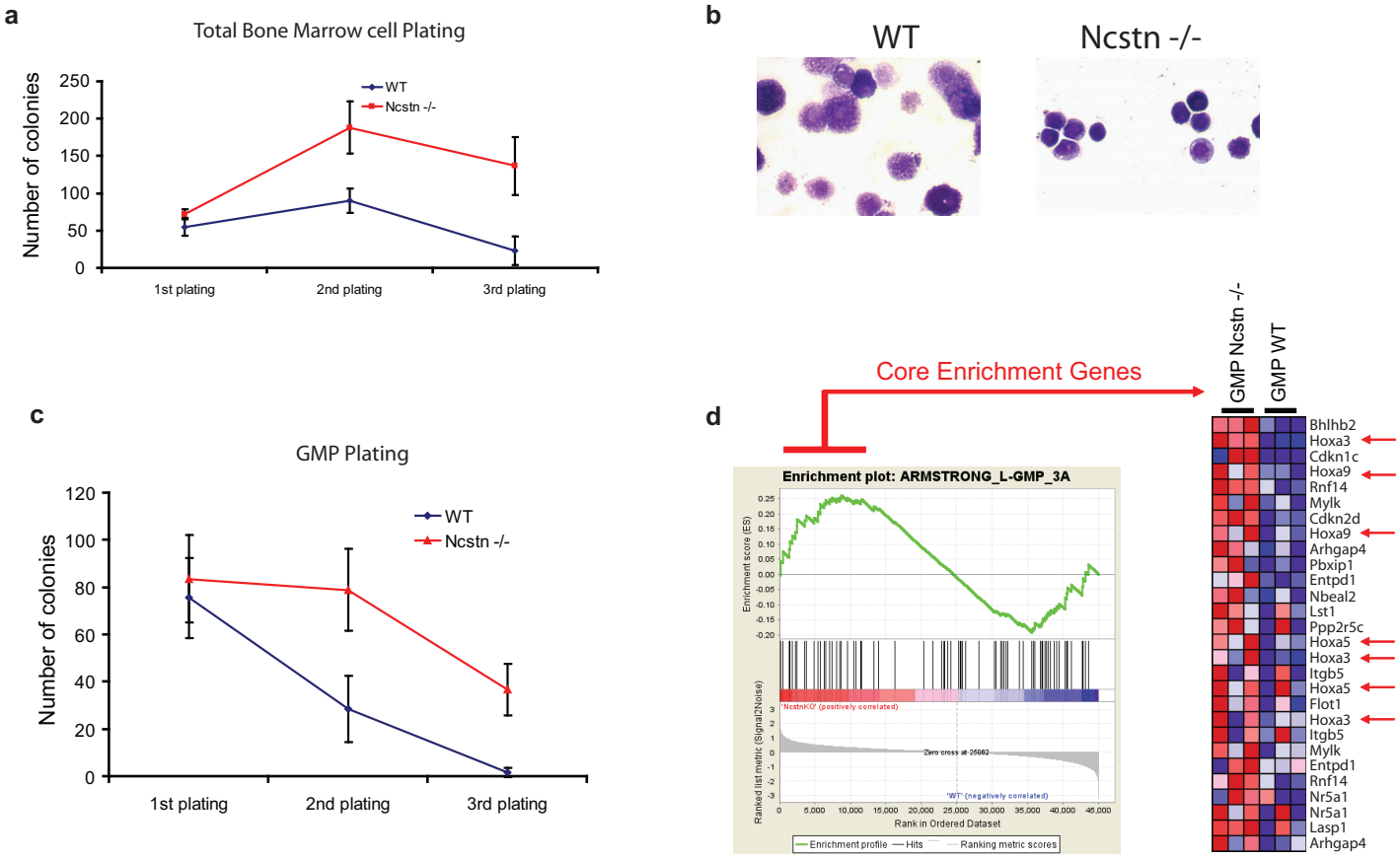

Supplemental Figure 6: Ncstn deletion increases the self-renewal potential of hematopoietic progenitors.

a, Plating of total bone marrow cells and 3 subsequent re-platings, using the same number of cells each time(15000 cells). Note the persistent re-plating of the Ncstn$^{f/f}$ vav1-cre+ cells compared to WT littermates (mean±S.D of 3 individual mice plated in triplicate). **b,** Cytospin and Wright-Giemsa staining of WT and Ncstn$^{f/f}$ Vav1-cre+ colonies after the 3rd re-plating. Note the differentiated WT cells and the undifferentiated, myeloblast-like morphology of the Ncstn$^{-/-}$ cells. **c,** An identical experiments as in a but the starting population is a sorted GMP (mean±S.D of 3 individual mice plated in triplicate). **d,** Microarray analysis comparing freshly purified GMP from Ncstn$^{-/-}$ and WT littermates. GSEA analysis showing enrichment of several of the core "L-GMP self-renewal gene signature" as defined by Krivtsov et al. Notice the upregulation of genes- members of the Hoxa family (arrows).

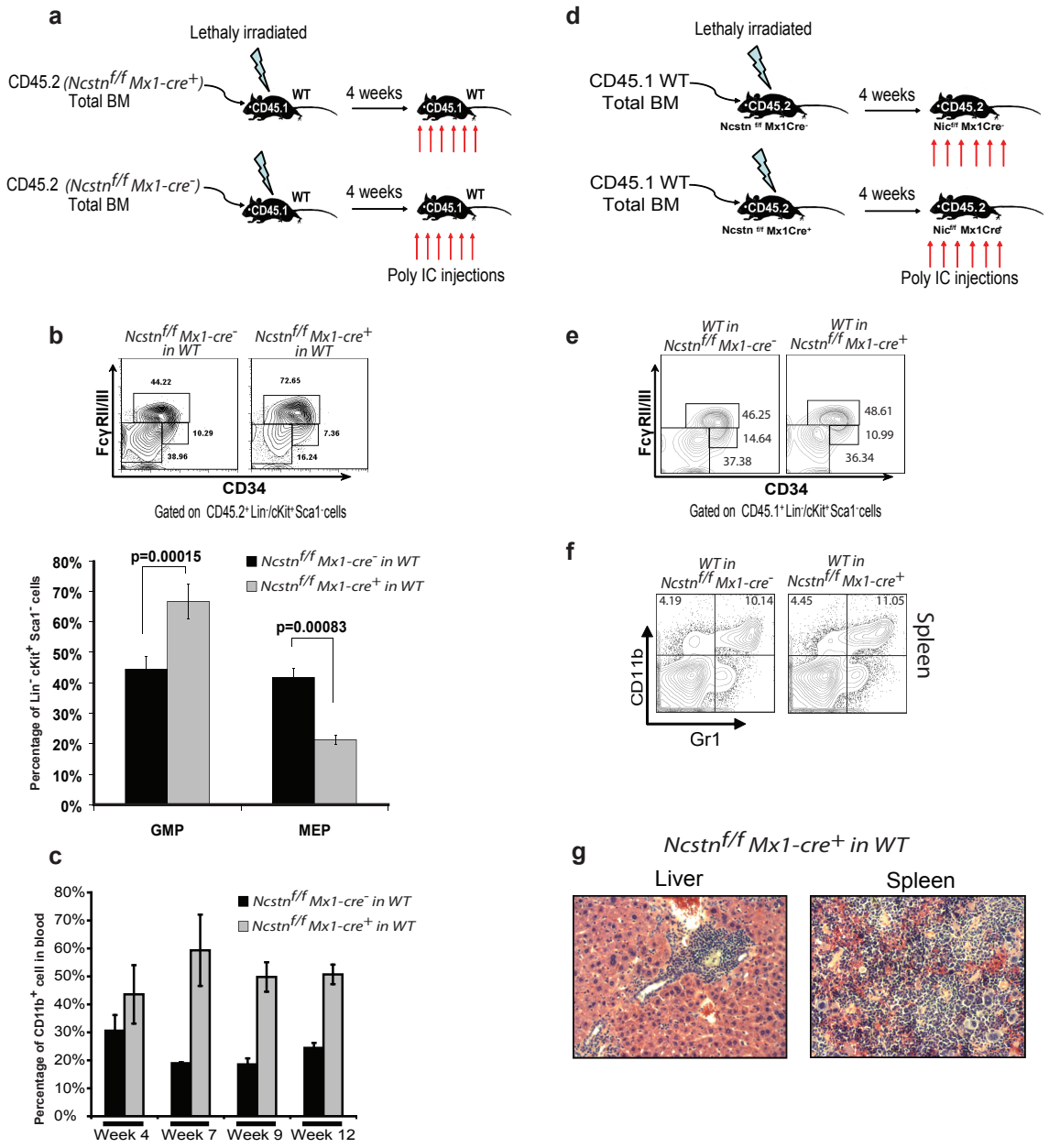

Supplemental Figure 7: The Ncstn deletion phenotype is cell-autonomous.
a, Bone marrow transplant strategy: CD45.2 total bone marrow cells from Ncstn$^{f/f}$ Mx1-cre+ or Ncstn$^{f/f}$ Mx1-cre- mice were transplanted in CD45.1 lethally irradiated WT recipients. 4 weeks after transplantation, recipients were injected with polyI-polyC. **b,** FACS analysis showing Myeloid Progenitors staining (upper panel) of bone marrow from representative mice transplanted with Ncstn$^{f/f}$ Mx1-cre+ or Ncstn$^{f/f}$ Mx1-cre- cells and bar graphs (lower panel) showing relative quantification of Granulocyte/Monocyte Progenitors and Megakaryocyte/Erythrocyte Progenitors (mean±S.D., Ncstn$^{f/f}$ Mx1-cre- n=4; Ncstn$^{f/f}$ Mx1-cre+ n=6). **c,** Bar graphs showing relative percentage of CD11b+ cells in peripheral blood of transplanted mice. **d,** Reverse bone marrow transplant strategy: CD45.1 WT total bone marrow cells were transplanted in CD45.2 lethally irradiated Ncstn$^{f/f}$ Mx1-cre+ or Ncstn$^{f/f}$ Mx1-cre- recipients. 4 weeks after transplantation, recipients were injected with polyI-polyC. **e,** FACS analysis showing Myeloid Progenitors staining of bone marrow from representative Ncstn$^{f/f}$ Mx1-cre+ or Ncstn$^{f/f}$ Mx1-cre- mice transplanted with WT bone marrow cells (mean±S.D., Ncstn$^{f/f}$ Mx1-cre- n=3; Ncstn$^{f/f}$ Mx1-cre+ n=3). **f,** Peripheral (spleen) FACS analysis of myeloid cells in the transplanted hosts. **g,** Hematoxylin and Eosin staining of liver and spleen sections from Ncstnf/f Mx1-cre+ progenitors transplanted in WT hosts.

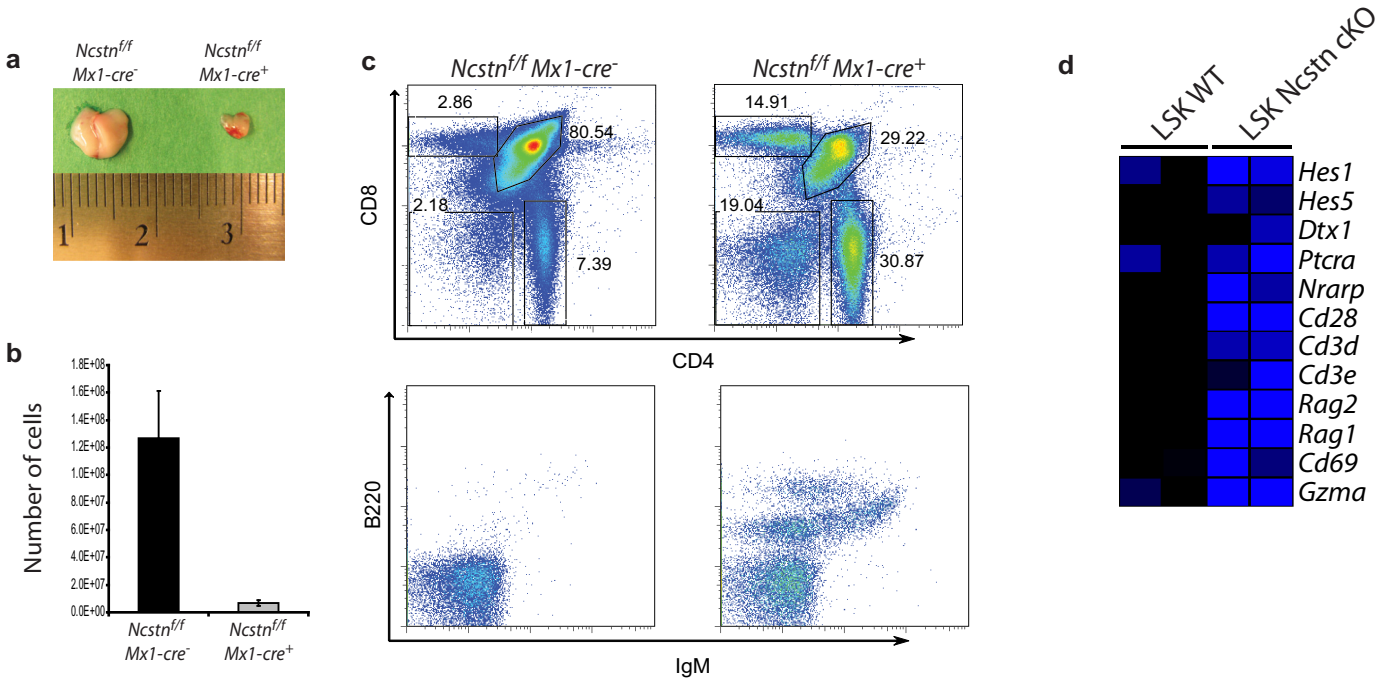

Supplemental Figure 8: Ncstn deletion suppresses Notch signaling and thymic T cell development
a, Ncstn$^{f/f}$ Mx1-cre+ mice showed a marked reduction in thymus size. Freshly isolated thymi from 6-weeks old Ncstn$^{f/f}$ Mx1-cre- (control) versus Ncstn$^{f/f}$ Mx1-cre+ mice. **b,** Bar diagram representing the average number of thymocytes in Ncstn$^{f/f}$ Mx1-cre- (control) and Ncstn$^{f/f}$ Mx1-cre+ mice. (mean±S.D., Ncstn$^{f/f}$ Mx1-cre- n=3; Ncstn$^{f/f}$ Mx1-cre+ n=3). **c,** Flow cytometric analysis of CD4/CD8 T cells and IgM/B220 B cells from thymus of 6-weeks-old Ncstn$^{f/f}$ Mx1-cre- (control) and Ncstn$^{f/f}$ Mx1-cre+ litter-mates. **d,** Heat map showing down-regulation of specific Notch target genes and T cell differentiation genes in LSK cells isolated from Ncstn$^{f/f}$ Mx1-cre+ compared to control LSK.

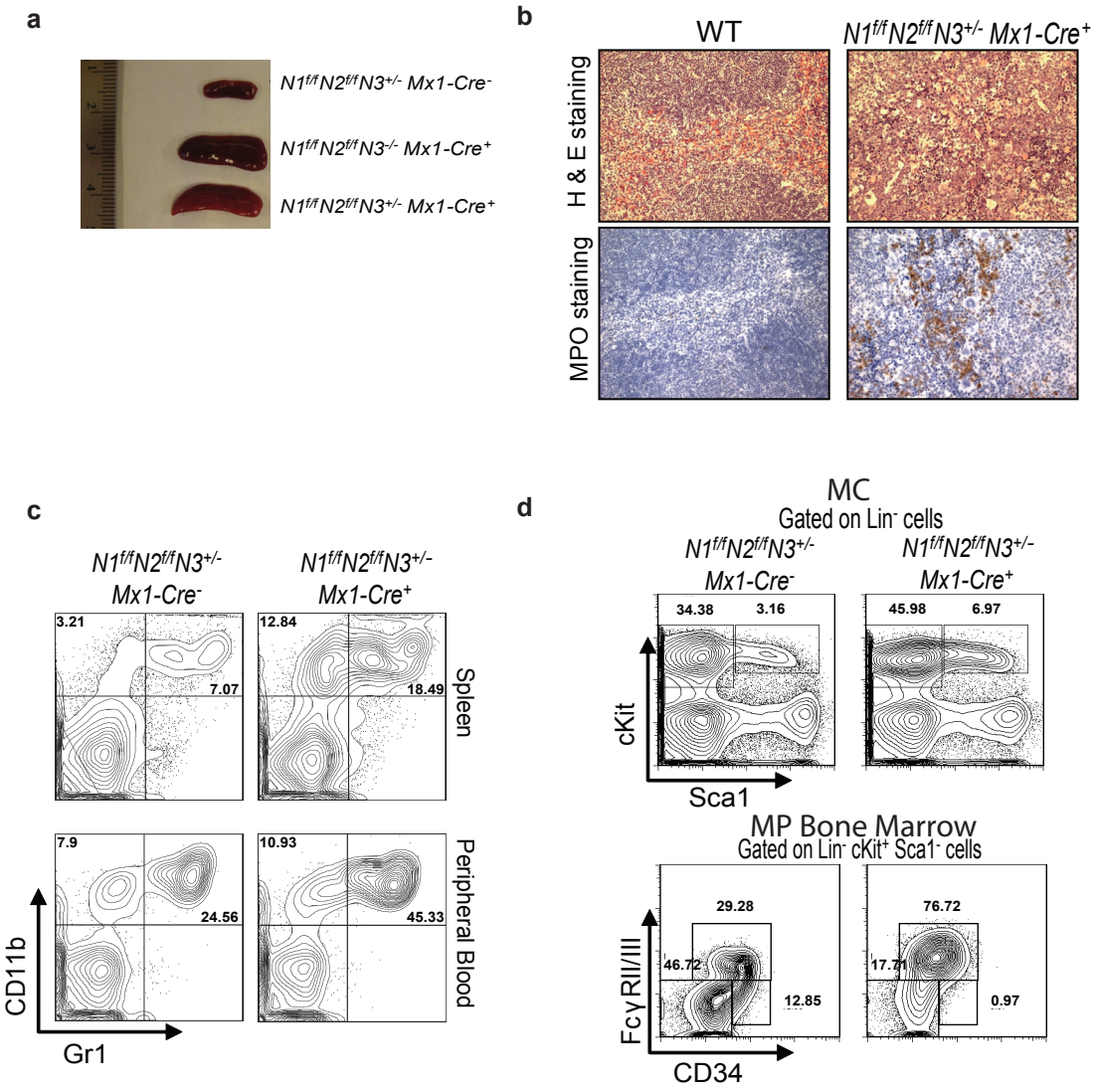

Supplemental Figure 9: The Notch pathway is a major γ-secretase target and is responsible for the Ncstn$^{-/-}$ phenotypes.

a, Myeloproliferative disease in N1$^{f/f}$ N2$^{f/f}$ N3$^{+/-}$ Mx1-cre+ mice. Relative spleen size is shown. b, H&E staining od spleen shows enlargement of red pulp and signs of extramedullary hematopoiesis (upper panel), Myeloperoxydase (MPO) staining of spleen sections shows massive invasion by myeloid cells (lower panel). c, Flow cytometric analysis of Gr1/CD11b myeloid cells from spleen and peripheral blood of 6-weeks-old N1$^{f/f}$ N2$^{f/f}$ N3$^{+/-}$ Mx1-cre+ and WT littermate. d, Detailed FACS analysis of bone marrow multipotent cells (MC: Lin-/c-Kit/Sca-1) and bone marrow myeloid progenitors (MP: Lin-/c-Kit+/Sca-1-/CD34/FcgRII/III) populations of WT and N1$^{f/f}$ N2$^{f/f}$ N3$^{+/-}$ Mx1-cre+ littermates.

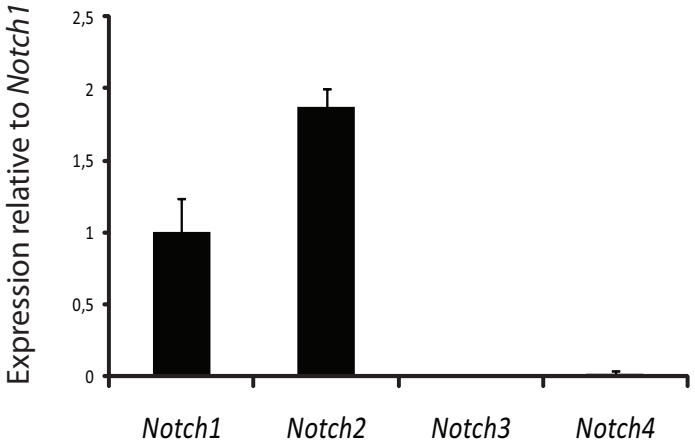

Supplemental Figure 10: Expression of Notch receptors by LSK cells.
RNA from LSK cells of WT mice were used to perform analysis of Notch1, Notch2, Notch3 and Notch4 gene expression using quantitative RT-PCR. Expression is normalized to Notch1. Mean ± SD of triplicate experiments is represented.

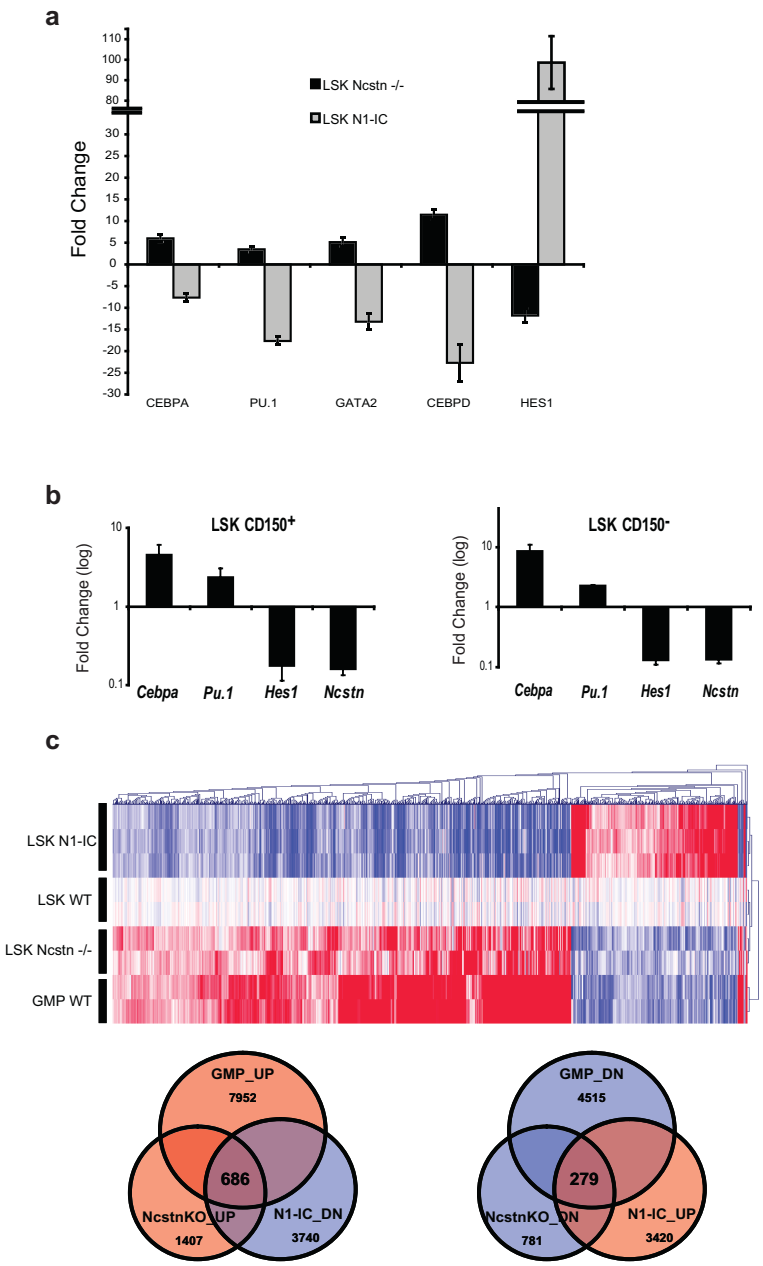

Supplemental Figure 11: Nsctn deficiency induces a de novo myeloid differentiation program in LSK cells. **a,** RNA from LSK cells of WT, Ncstn$^{f/f}$ Mx1-cre+ and lsl-N1-IC Mx1-cre+ mice were used to perform analysis of Hes-1, Cebpa, Gata2, Pu.1 and Cebpd genes using quantitative RT-PCR. Expression is normalized to WT cells. Mean ± SD of triplicate experiments is represented. **b,** cDNA from LSK CD150+ or LSK CD150- cells of WT and Ncstn$^{f/f}$ Mx1-cre+ littermates were used to perform analysis of Cebpa, Pu.1, Hes-1 and Ncstn genes using quantitative RT-PCR. Expression is normalized to control WT expression level. Mean ± SD of triplicate experiments is represented. **c,** Heat map of genes significantly up or down regulated in Ncstn$^{-/-}$ LSK, that follow the same pattern of expression in WT GMP and the opposite pattern in LSK N1-IC. Expression level is normalized to expression in LSK WT (upper panel). Venn diagram showing number of genes significantly up or down regulated in Ncstn$^{-/-}$ LSK, that follow the same pattern of expression in WT GMP and the opposite pattern in LSK N1-IC (lowe panel).

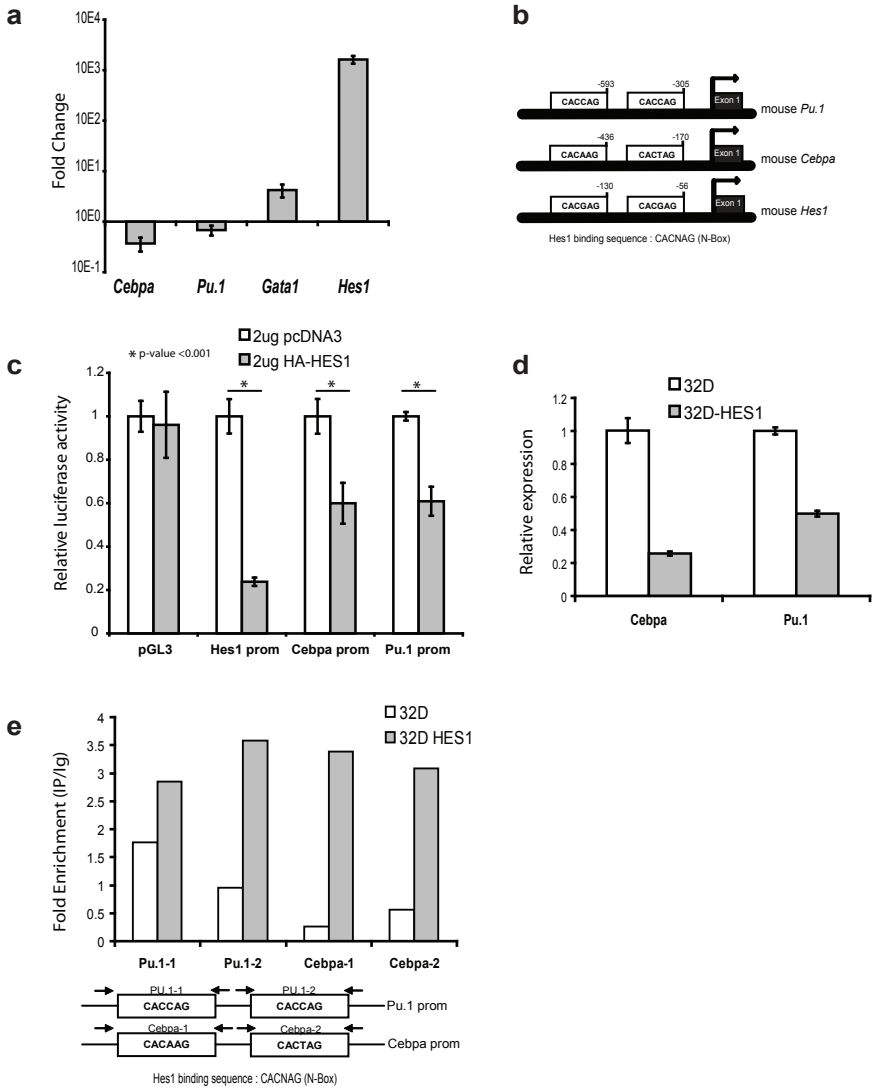

Supplemental Figure 12: HES1 suppresses granulocyte/monocyte differentiation by binding Cebpa and Pu.1 promoters.

a, Selected Lineage negative cKit+ bone marrow cells from WT mice were transduced with retroviruses encoding Hes-1 or empty vector and subsequently grown in liquid culture supplemented with cytokines. 48h after infections, infected GFP+ cells were sorted and expression of genes was assessed by quantitative RT-PCR. Expression is normalized to control infected cells. Mean ± SD of three experiments is represented. **b,** Schematic representation of mouse Pu.1, Cebpa and Hes1 promoters showing the presence of putative Hes1 binding sequences (N-Box). **c,** HEK293T cells were transfected with pGL3prom empty vector or pGL3prom vector containing Pu.1, Cebpa or Hes1 promoter sequence together with pcDNA3 empty vector or a vector allowing expression of HA-tagged HES1 and Renillia expressing vector. Luciferase and Renilla activities were examined 24 hours after transfection. To compare HES1 repression on promoter constructs, promoter activities in HA-HES1 transfected cells were expressed as the percentage of those in pcDNA transfected cells. Luciferase activity is normalized over Renillia activity. The data represent the averaging of three independent experiments performed in duplicates. **d,** Quantitative RT-PCR analysis of Cebpa and Pu.1 genes in 32D cells infected by empty retroviral vector or retroviral vector encoding HES1. **e,** ChIP assay for Hes1 binding on the promoters of Pu.1 and Cebpa in 32D cell line einfected by empty retroviral vector or retroviral vector encoding HES1. Fold enrichment (IP/Ig control) is shown. In the lower panel, location of the primer is shown. A representative of three identical experiments is shown.

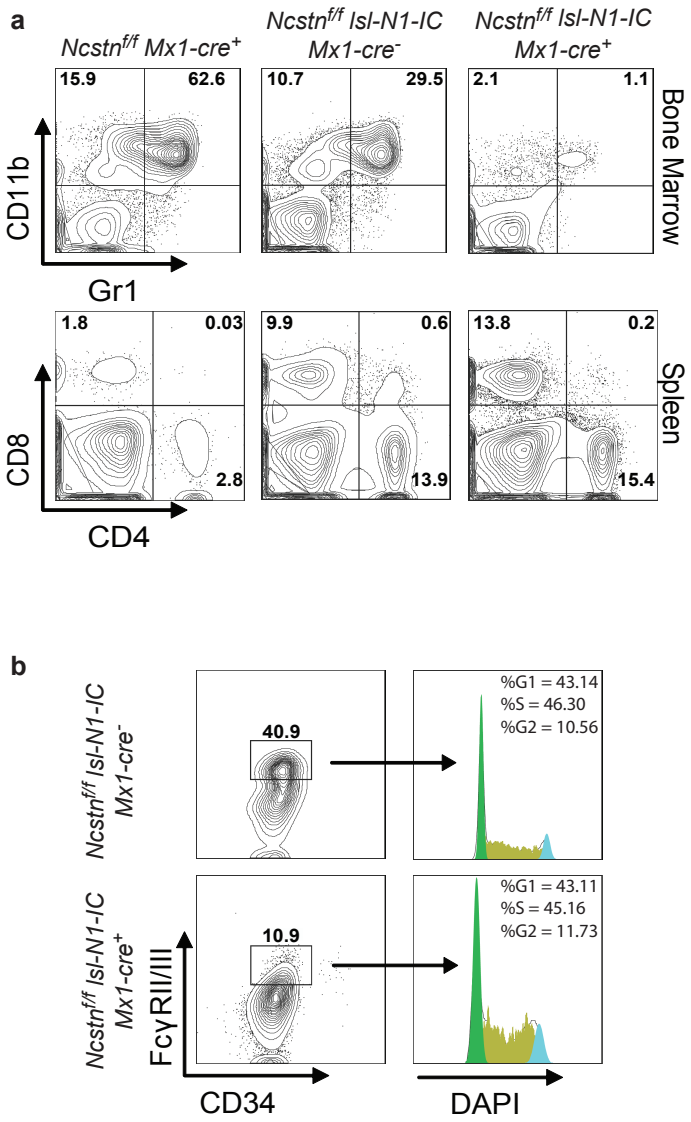

Supplemental Figure 13: Ectopic expression of Notch1IC is able to suppress CMML-like disease in Ncstn$^{-/-}$ mice.

a, PolyI-polyC-induced Notch1-IC expression in Ncstn$^{f/f}$ lsl-N1-IC Mx1-Cre+ animals suppresses the generation of myeloid cells in the bone marrow. Also the relative effects of the expression of Notch1-IC on the peripheral T cell compartment (spleen) are shown (n=5 mice from each genotype). **b,** Unchanged cell cycle status of GMP cells from polyI-polyC treated Ncstn$^{f/f}$ lsl-N1-IC Mx1-Cre+ or control littermate animals,

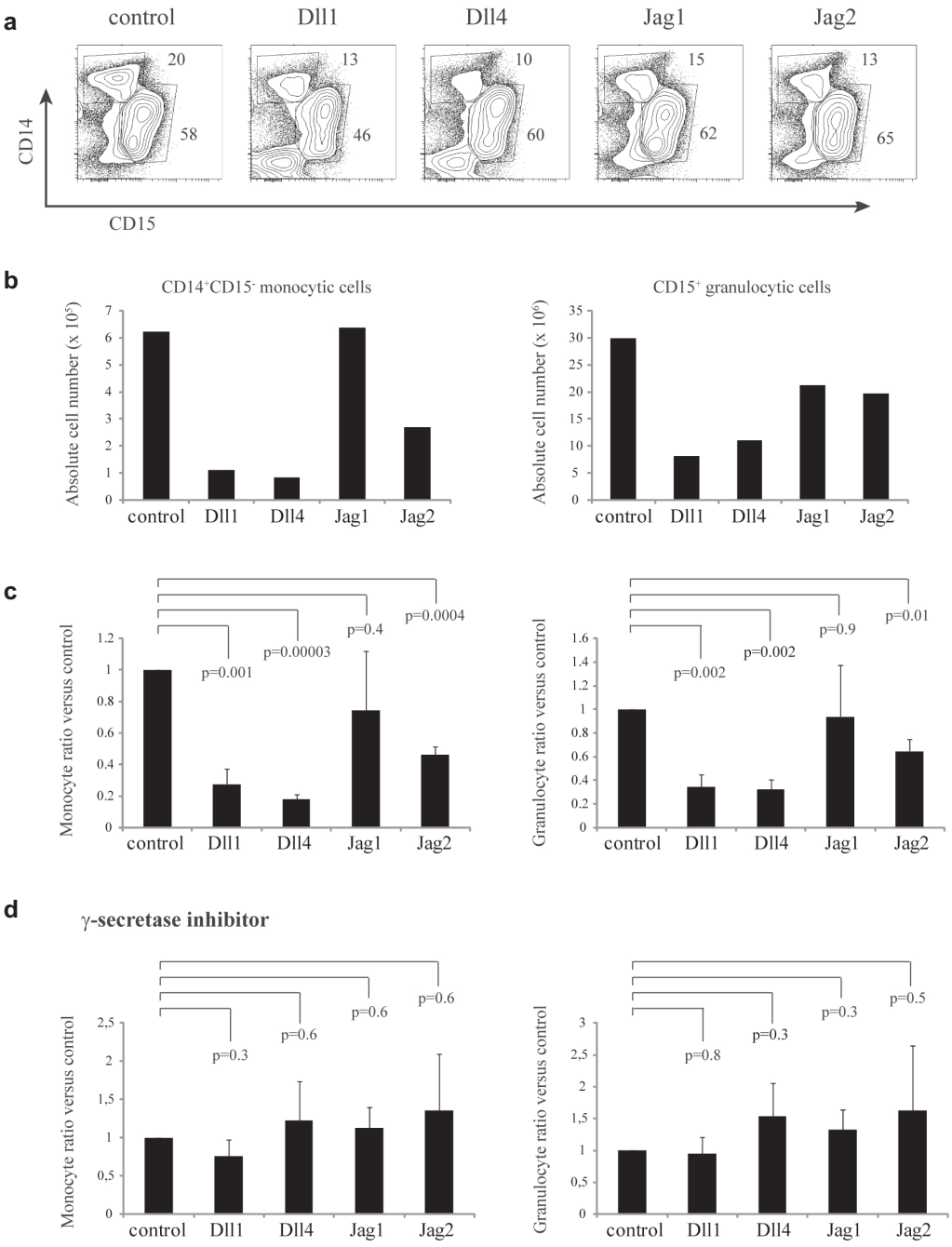

Supplemental Figure 14: Human myelopoiesis is suppressed by activation of Notch signaling. **a,** Flow cytometric analysis of human CD45+ gated CD14/CD15 myeloid differentiation after OP9 co-culture of human bone marrow CD34+CD38-Lin- hematopoietic precursor cells in the absence or presence of different Notch ligands. **b,** Bar diagram of one representative experiment indicating the absolute number of human CD14+CD15- monocytic cells (left diagram) and CD15+ granulocytic cells (right diagram) from OP9 cocultures in a. **c,** Bar diagram of the average ratio of human CD14+CD15- monocytic cells (left diagram) and CD15+ granulocytic cells (right diagram) generated in each OP9 co-culture condition versus the control co-culture (mean±S.D., n=4). **d,** Addition of γ-secretase inhibitor inhibits the ability of Notch ligands to suppress myelopoiesis (mean±S.D., n=4).

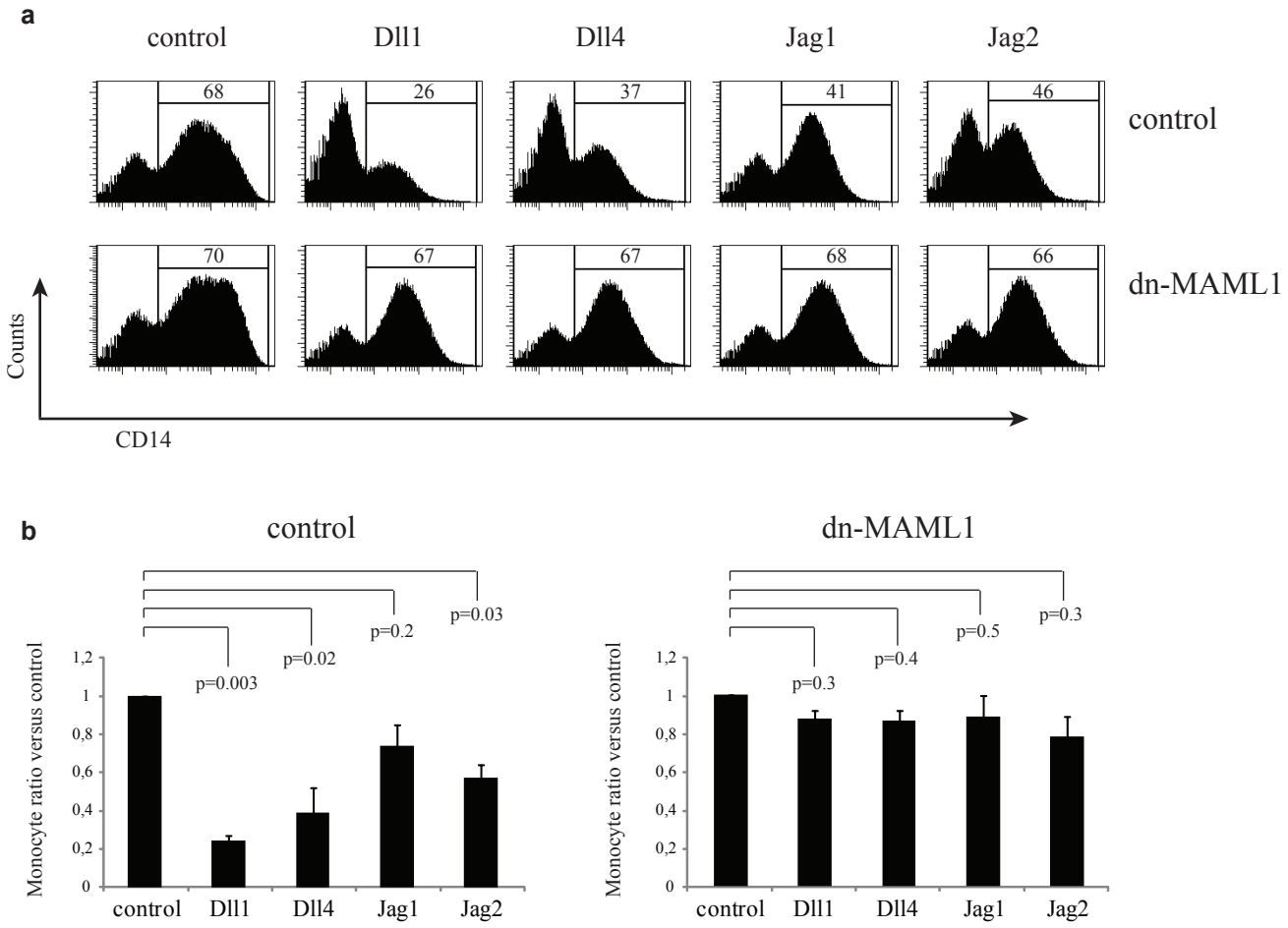

Supplemental Figure 15. Notch pathway silencing through the expression of a mutated MAML1 inhibits pathway ability to suppress differentiation of human monocytes.
a, FACS analysis showing the reversal of the monocytic inhibition by infecting the CD34+38- cord blood stem and progenitor cells with a mutated dominant negative MAML1 (dnMAML1) or an EGFP-only control. **b,** Quantification of the experiment showed in Panel A (mean±S.D., n=3).

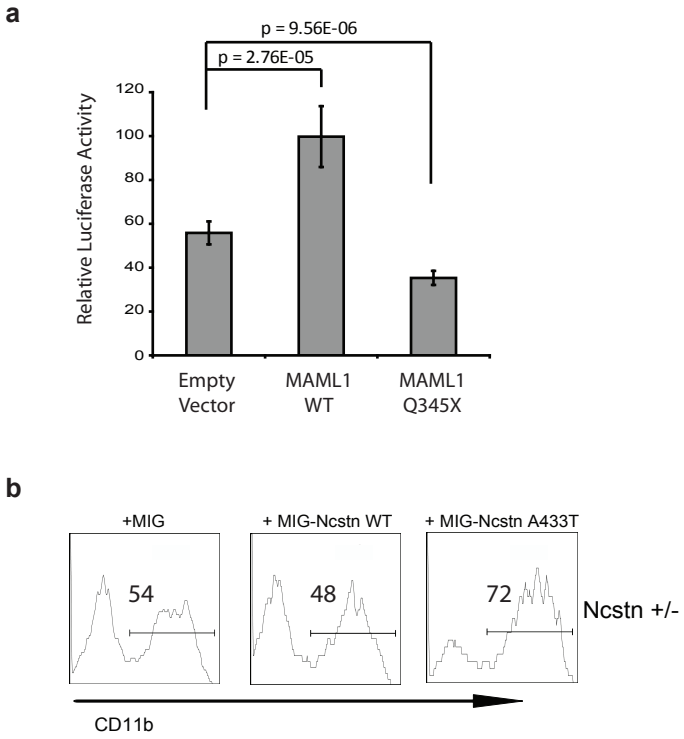

Supplemental figure 16: MAML1 Q345X and NCSTN A433T mutant have dominant negative potential.

a, Notch luciferase reporter assay in 239T cells transfecting the cells with either empty vector, WT MAML1 or MAML1 Q345X together with N1-IC and renillia expressing vector. Dual luciferase intensities are measured 24h after transfection (mean±S.D., n=3).

b, OP9-DL1 co-culture of $Ncstn^{+/-}$ LSK cells ($Ncstn^{f/wt}$ vav1-cre+) infected with specified constructs. Analysis of CD11b+ population was studied 14 days after the initiation of the culture. A representative of 3 independant experiments is shown

Supplemental Table 1: GSEA on expression datasets of LSK from *Ncstn$^{f/f}$ Mx1-cre^{+}* mice versus LSK from WT mice.

GeneSets	SIZE	ES	NES	p-value	FDR	References
MYELOID_SIGNATURE	67	0.78	**2.71**	<0.001	<0.001	
LIAN_MYELOID_DIFF_GRANULE	39	0.71	**2.21**	<0.001	<0.001	(Lian et al., 2001)
LIAN_MYELOID_DIFF_RECEPTORS	64	0.57	**1.95**	<0.001	<0.001	(Lian et al., 2001)
LIAN_MYELOID_DIFF_TF	75	0.45	**1.56**	0.011	0.023	(Lian et al., 2001)
MYELOID_LEUKOCYTE_DIFFERENTIATION	38	0.47	**1.43**	0.067	0.056	(Ashburner et al., 2000)
MYELOID_CELL_DIFFERENTIATION	81	0.34	**1.21**	0.176	0.179	(Ashburner et al., 2000)

Genesets are defined from the indicated publications and available at http://www.broad.mit.edu/gsea
ES= Enrichment Score
NES= Normalized Enrichment Score
FDR= False Discovery Rate

Lian, Z *et al.* Genomic and proteomic analysis of myeloid differentiation program. *Blood* **98**, 513-524 (2001)
Ashburner, M. *et al.* Gene ontology: tool for the unification of biology. The Gene Ontology Consortium. *Nat Genet* **25**, 25-29 (2000)

Supplemental Table 2: GSEA on expression datasets of LSK from *N1-IC*$^{+}$ *Mx1-cre*$^{+}$ mice versus LSK from WT mice

GeneSets	SIZE	ES	NES	p-value	FDR	References
MYELOID_SIGNATURE	67	-0.77	**-2.29**	<0.001	<0.001	
LIAN_MYELOID_DIFF_GRANULE	39	-0.79	**-2.10**	<0.001	<0.001	(Lian et al., 2001)
LIAN_MYELOID_DIFF_RECEPTORS	64	-0.51	**-1.49**	0.018	0.036	(Lian et al., 2001)
LIAN_MYELOID_DIFF_TF	75	-0.40	**-1.22**	0.142	0.210	(Lian et al., 2001)
MYELOID_LEUKOCYTE_DIFFERENTIATION	38	-0.38	**-1.02**	0.419	0.410	(Ashburner et al., 2000)

Genesets are defined from the indicated publications and available at http://www.broad.mit.edu/gsea
ES= Enrichment Score
NES= Normalized Enrichment Score
FDR= False Discovery Rate

Supplemental Table 3: Clinical characteristics of CMML patients.

SAMPLE ID	Sex	Age	Diagnosis	Peripheral WBC[a] count (x10^9/uL)	Peripheral Monocytosis (x10^9/uL)	BM Blast (%)	BM Monocyte (%)	\CG Karyotype
7	F	64	CMML-1	25.4	6.4	5	12	46, XX inv(3)(q21q26.2) in 14 metaphases and 46 XX inv(3)(q21q26.2), -7 in 6 metaphases
8	F	60	CMML-2	11.7	1.1	16	12	47, XX, +8 (in 17 metaphases)
10	M	66	AML transformed from CMML	129.4	9.1	22	9	47, XY +21 (in 6 metaphases), 47, XY, +15 (in 1 metaphase)
19	F	55	CMML-1	30.4	7	4	13	46, XX
817	M	65	CMML-1	11.8	4.5	4	12	46, XY
1	M	61	CMML-1	9.4	5.1	1	9	ND
2	M	50	CMML-1	5.2	1.2	1	3	(19)46XYDER(15)T(1;15)(Q11;P13)
3	M	76	CMML-1	43	7.3	2	15	(20)46XY
4	M	60	CMML-1	6.8	1.6	2	5.8	ND
5	M	66	CMML-1	41.4	5.8	2	4	46,XY,t(13;14)(q12;q32)[20]
6	M	62	CMML-1	24.8	4.2	2	4	46,XY,del(7)(p15){20}
9	M	55	CMML-1	5.1	2.1	3	7	46 XY [20]
11	M	69	CMML-1	3.9	1.7	4	8	(20)46XY
12	M	76	CMML-1	36.5	8.4	4	13	46,XY{20}
13	M	58	CMML-1	10	2	4	14	46,XY{20}
14	M	55	CMML-1	30.4	7	4	13	(20)46XY
15	F	73	CMML-1	28.9	6.1	5	5	27)46XX
16	M	67	CMML-1	28.8	2.9	5	1	46,XY{20}
17	M	77	CMML-1	7.6	3.1	5	8	46,XY,{20}
18	M	33	CMML-1	74	17	5	12	(4)47XY,+10;(16)DIP
20	M	73	CMML-1	6.7	3	5	16	14)45XY-7,DEL(12)(P11);6)DIP
21	M	58	CMML-1	25.7	5.7	5	12	20)46XY
22	M	64	CMML-1	59.5	13.7	5.2	14.2	(20)46XY
23	F	65	CMML-1	37.9	7.6	6	8	46,XX[20]
24	M	66	CMML-1	97.6	43.9	6	27	(20)46XY
25	F	49	CMML-1	99	14.9	6	6	46,XX {20}
26	M	70	CMML-1	90.7	47.2	7	42	(12)46XY
27	M	73	CMML-1	18.6	5	7.2	8.4	(18)45XY-7;(2)DIP
28	M	71	CMML-1	48.9	2.4	8	15	3)46XYDEL(13)(Q12;Q14);17)DIP
29	M	75	CMML-1	30.8	5.5	8	13	(19)46XY
30	M	66	CMML-1	2.6	0.8	9	25	(20)46XY
31	F	68	CMML-2	48.9	22	10	21	(20)46XX

32	M	68	CMML-2	11.8	5.8	11	24	(20)45XY,-7,DEL12(P12.3)
33	F	62	CMML-2	40	9.2	11	18	20)47XX+8
34	M	68	CMML-2	40.2	10.5	13	28	46,XY{19}
35	M	54	CMML-2	87.3	40.2	13	40	(27)46XY
36	M	66	CMML-2	6.9	1.3	14	3	45,XY,-7[16]; 45,XY,ins(1;?) (p34;?),-7[3]; 45,XY,-7,del(12)(p12)[1]
37	F	67	CMML-2	21.7	3.9	16	11	45,XX,-7{17};46,XX{3}
38	M	50	CMML-2	12.4	2.5	16	10	(30)46XY,INV9(P11Q12)
39	M	65	CMML-2	2.9	1.1	16	14	(21)46XY
40	M	75	CMML-2	19.1	6.1	19	10	46,XY [20]
41	M	31	CMML-2	34.4	17.5	missing	missing	46,XY[20]

[a]WBC: White Blood Cells

Supplemental Table 4: Notch pathway mutations founf in CMML patients and co-occuring mutations

ID	Sex	Age	Diagnosis	Notch pathway mutations	Co-occuring mutations						
					IDH1	IDH2	TET2	ASXL1	FLT3	N/K-RAS	JAK2
7	F	64	CMML-1	*APH1A V194I*	WT	WT	R1962H	WT	WT	K-RASG12D	V617F
8	F	60	CMML-2	*NOTCH2 S879F*	WT	WT	WT	WT	WT	WT	WT
10	M	66	AML transformed from CMML	*MAML1 R783W NCSTN T304I*	WT	WT	L1667fsX 23	E322X; E635RfsX14	WT	WT	WT
19	F	55	CMML-1	*NCSTN A433T*	WT	WT	C1877R	H995QfsX2	WT	N-RASG12D	WT
817	M	65	CMML-1	*MAML1 Q345X*	WT	WT	Q958X	E635RfsX14	WT	WT	WT

All coding regions of IDH1, IDH2, TET2, ASXL1, APH1A, MAML1, PEN2, PRESENILIN1/2, NICASTRIN, NOTCH1, and NOTCH2 were sequenced as well as regions of previously described mutations in JAK2, KRAS, NRAS, and FLT3.

Supplemental Table 5: Single nucleotide variants found in CMML patients.

Gene	Alteration
APH1A	V255A
MAML1	N114S
MAML1	N501S
MAML1	S508F
MAML1	G950S
Nicastrin	E109G
Notch1	C74R
Notch1	F345L
Notch1	D388G
Notch1	K581R
Notch1	I659V
Notch1	G691S
Notch1	S759F
Notch1	S1274F
Notch1	L1580Q
Notch1	V1579M
Notch 2	T696A
Notch 2	A1108V

(They may represent somatic missense mutations or unannotated SNPs due to the fact that the variant was seen in tumor DNA but no matched normal DNA was available).